Altered development in GABA co-release shapes glycinergic synaptic currents in cultured spinal slices of the SOD1^{G93A} mouse model of ALS

Manuela Medelin[1], Vladimir Rancic[1], Giada Cellot[1], Jummi Laishram[1], Priyadharishini Veeraraghavan[2], Chiara Rossi[3], Luca Muzio[3], Lucia Sivilotti[4] & Laura Ballerini[1,2*]

[1] Department of Life Sciences, University of Trieste, 34127 Trieste, Italy.
[2] International School for Advanced Studies (SISSA/ISAS), 34136 Trieste, Italy.
[3] Neuroimmunology Unit, Division of Neuroscience, Institute of Experimental Neurology (INSPE), San Raffaele Scientific Institute, 20132 Milan, Italy.
[4] Department of Neuroscience, Physiology and Pharmacology, University College London (UCL), London WC1E 6BT, England, UK.

Running title: Inhibitory inputs in the SOD1^{G93A} spinal cord

Key Words: organotypic cultures; glycinergic currents; spinal interneurons; neurodegenerative disease

***Corresponding author**: Laura Ballerini: International School for Advanced Studies (SISSA/ISAS), via Bonomea 265 I-34136 Trieste, Italy, Email laura.ballerini@sissa.it

Table of Contents category: Neuroscience, neurobiology of disease

Key points summary:

- Increased environmental risk factors in conjunction with genetic susceptibility has been proposed in Amyotrophic lateral sclerosis (ALS) remarkable variations in mortality
- In vitro models allow investigating genetically modified counter-regulator of motoneuron toxicity and might help in addressing ALS therapy
- Spinal organotypic slice cultures from SOD1^{G93A} mouse model of ALS allow us to detect altered glycinergic inhibition in spinal microcircuits
- This altered inhibition improved spinal cord excitability affecting motor outputs in early SOD1^{G93A} pathogenesis

Abstract

Amyotrophic lateral sclerosis (ALS) is a fatal, adult-onset neurological disease characterized by progressive degeneration of motoneurons (MNs). In our previous study we developed organotypic spinal cultures from an ALS mouse model expressing a mutant form of human superoxide dismutase 1 ($SOD1^{G93A}$). We reported the presence of a significant synaptic rearrangement expressed by these embryonic cultured networks, which may lead to altered development of spinal synaptic signalling, potentially linked to the adult disease phenotype. Recent studies on the same ALS mouse model, reported a selective loss of glycinergic innervation in cultured MNs, suggestive of a contribution of synaptic inhibition to MNs dysfunction and degeneration. Here we further exploit organotypic cultures from wild type and $SOD1^{G93A}$ mice to investigate the development of glycine-receptor mediated synaptic currents recorded from interneurons of the premotor ventral circuits. We perform single cell electrophysiology, immunocytochemistry and confocal microscopy and we suggest that GABA co-release may speed the decay of glycine responses altering, in $SOD1^{G93A}$ developing networks, temporal precision and signal integration at the postsynaptic site. Our hypothesis is supported by the finding of an increased MN bursting activity in immature $SOD1^{G93A}$ spinal cords and by immunofluorescence microscopy detection of longer persistence of GABA in $SOD1^{G93A}$ glycinergic terminals in cultured and ex-vivo spinal slices.

Abbreviations

ALS, Amyotrophic lateral sclerosis; DRG, dorsal root ganglia; mPSCs, miniature glycinergic currents; MNs, motoneurons; gly-PSCs, glycine-receptor mediated synaptic currents; PSC, post synaptic current; RT, room temperature; $SOD1^{G93A}$, mutant form of human superoxide dismutase 1; VR, ventral root; WIV, weeks in vitro; WT, wild type;

Introduction

Familial and sporadic forms of amyotrophic lateral sclerosis (ALS) are characterized by progressive degeneration of upper and lower motoneurons (MNs; Ling et al., 2013). Many diverse disease mechanisms have been proposed (Rothstein, 2009), focusing most recently on specific alterations in protein- and/or ribonucleic-metabolic pathways (Robberecht & Philips, 2013), a hypothesis supported by genetic analysis, including exome sequencing in sporadic ALS (Cirulli et al., 2015). Nevertheless, it is still unclear how different molecular pathologies determine two important features of ALS: the great variability in the time of disease onset and the selective vulnerability of MNs, with variable patterns across MN pools in the spinal cord (Robberecht & Philips, 2013).

Around 20% of familial ALS cases are associated with mutations in the superoxide dismutase 1 (SOD1 OMIM*147450) gene. Transgenic mice expressing additional copies of the human mutant gene are good models of adult-onset ALS (McGoldrick et al., 2013). These display neurodegenerative processes mimicking human ALS and are the most widely used models to investigate the molecular pathways correlated to the disease onset (Rothstein, 2003; Turner & Talbot, 2008). A strong case can be made for investigating ALS and other neurodegenerative processes in immature neuronal networks, in order to capture pre-symptomatic alterations in synaptic signalling (Ben-Ari, 2008). It has recently been reported that spinal synaptic inhibition is insufficient in mice expressing a mutated human SOD1, $SOD1^{G93A}$ (Chang & Martin, 2009, 2011; Martin & Chang, 2012). Cultured $SOD1^{G93A}$ MNs display selective loss of glycinergic innervation, when compared with age-matched wild type (WT) MN (Chang & Martin, 2011). Using organotypic cultures from mouse spinal cords to model network development (Avossa et al., 2003; Rosato-Siri et al., 2004; Furlan et al., 2007), we reported in mutant $SOD1^{G93A}$ imbalance between synaptic excitation and inhibition and an increased MN susceptibility to mild excitotoxic stressors *in vitro* (Avossa et al., 2006). However, it is unknown how the spatio-temporal expression of the

glycinergic/GABAergic system and its contribution to early pre-motor network function is affected during spinal maturation in SOD1^{G93A} mice.

Here we further exploit organotypic cultures from wild type (WT) and SOD1^{G93A} mice to investigate glycine-receptor mediated post synaptic currents (gly-PSCs). We found that the speeding up of the decay phase of gly-PSCs with spinal maturation was greater in SOD1^{G93A} interneurons than in WT, despite the broadly similar properties of glycinergic single channel activity in age-matched WT and SOD1^{G93A} patches. The most likely explanation for the difference in gly-PSC decay may be that SOD1^{G93A} synapses retain greater GABA co-expression and co-release than WT, a hypothesis supported by our observation of the effects of depleting glycinergic terminals of GABA and by immunofluorescence microscopy detection of GABA in glycinergic terminals. The influence of the greater GABA co-localization on spinal integrated motor outputs was examined using isolated WT and SOD1^{G93A} neonatal spinal cords via multiple ventral roots (VR) recordings. In developing SOD1^{G93A} spinal cords, spontaneous bursting events in VR recordings were longer than in WT. When this activity was recorded in the presence of a $GABA_A$ receptor antagonist, we also detected in SOD1^{G93A} spinal networks an enhanced excitation, characterized by faster bursting. Thus more persistent GABA co-release may affect, in SOD1^{G93A} developing networks, temporal precision and signal integration at postsynaptic site.

Methods

Preparation of spinal tissue cultures and isolated spinal cords

Transgenic mice (SOD1^{G93A}) expressing a high copy number of the glycine 93 to alanine mutation of the hSOD1 gene (B6SJL-TgN(SOD1-G93A)1Gur; Gurney et al., 1994) and non transgenic females (B6SJLF1) were purchased from the Jackson Laboratories (Bar Harbor, ME, USA) and bred as previously reported (Avossa et al., 2006). The wild type SOD1^{G93A} littermates (WT) were used as negative controls for the genetic background (Holasek et al., 2005; Schutz et al., 2005; Copray et al., 2003; Rao et al., 2003). Genotyping was determined by PCR analysis as previously

reported (Avossa et al., 2006). Briefly, organotypic slice cultures of spinal cord and dorsal root ganglia (DRG) were obtained from mouse embryos at days 12-13 of gestation as previously described (Avossa et al., 2003, 2006; Furlan et al., 2005, 2007; Rosato-Siri et al., 2004). Experiments were performed on WT and $SOD1^{G93A}$ sister cultures at 1, 2 and 3 weeks *in vitro* (WIV).

For the preparation of acute WT and $SOD1^{G93A}$ spinal slices, mice were sacrificed at P0 by cervical dislocation and spinal cords were collected in ice-cold PBS as previously described (Nigro et al., 2012), then fixed in 4% formaldehyde (prepared from fresh paraformaldehyde, Sigma) in PBS, pH 7.2 for 6 h at 4°C. Spinal cords were cryoprotected in PBS-30% Sucrose (Sigma) and then embedded in Optical Cutting Temperature (OCT; Bio-Optica) inclusion media. Samples were stored at -80° C before sectioning at 12 microns.

For ventral roots recordings, the entire spinal cords were isolated from WT and $SOD1^{G93A}$ neonatal mice (P2-P4) as previously reported (Bracci et al., 1996; Beato & Nistri, 1999; Taccola et al., 2008; Veeraraghavan & Nistri 2015). Briefly, animals were decapitated, internal organs were removed and a laminectomy was performed in order to expose and remove the spinal cord. Preparations were continuously superfused with standard Krebs solution containing (in mM): 113 NaCl, 4.5 KCl, 1 $MgCl_2.7H_2O$, 2 $CaCl_2$, 1 NaH_2PO_4, 25 $NaHCO_3$, 11 glucose, gassed with 95% O_2 and 5% CO_2 (pH 7.4) at room temperature (RT).

Genotyping was performed after the electrophysiological experiments had been performed in order to allow the electrophysiological experimenter to be “blind” to animal genotype. PCR analysis was then performed as reported (Avossa et al., 2006).

Ethical Statement

All experiments were performed in accordance with the EU guidelines (2010/63/UE) and Italian law (decree 26/14) and were approved by the local authority veterinary service and by our institution (SISSA-ISAS) ethical committee. All efforts were made to minimize animal suffering

and to reduce the number of animal used. Animals use was approved by the Italian Ministry of Health, in agreement with the EU Recommendation 2007/526/CE.

Electrophysiological recordings

For patch clamp recordings (whole-cell, voltage clamp mode) a coverslip with the spinal culture was positioned in a recording chamber, mounted on an inverted microscope, and superfused with control physiological saline solution containing (in mM): 152 NaCl, 4 KCl, 1 $MgCl_2$, 2 $CaCl_2$, 10 HEPES and 10 glucose. The pH was adjusted to 7.4 with NaOH (osmolarity 305mOsm). Cells were patched with pipettes (4-7 MΩ) filled with a solution of the following composition (in mM): 120 K gluconate, 20 KCl, 10 HEPES, 10 EGTA, 2 $MgCl_2$, 2 Na_2ATP. The pH was adjusted to 7.3 with KOH (295mOsm). All electrophysiological recordings were performed at RT.

Voltage values indicated in the text and in figures are corrected for the liquid junction potential (-14 mV) if not otherwise indicated. Series resistance value was <10 MΩ enabling recordings of synaptic currents without significant distortion, thus was not compensated for (Streit et al., 1991; Furlan et al., 2007). Recordings were performed from ventrally located spinal interneurones identified on the basis of previously reported criteria (Ballerini & Galante, 1998; Ballerini et al., 1999; Galante et al., 2000). Electrophysiological responses were amplified (EPC-7, HEKA; Multiclamp 700B, Axon Instruments), sampled and digitized at 10 kHz with the pCLAMP software (Axon Instruments) for offline analysis. Single spontaneous synaptic events were detected by the use of the AxoGraph X (Axograph Scientific) event detection program (Clements & Bekkers, 1997) and by the Clampfit 10 software (pClamp suite, Axon Instruments). On average, ≥ 400 events were analysed from each cell in order to obtain mean kinetic and amplitude parameters. From the average of these events we measured the rise time defined as the 10–90% time needed to reach the peak of the synaptic current, the peak amplitude and the decay time constant (expressed as τ) by fitting a mono-exponential function.

We detected no differences between WT (n=56) and $SOD1^{G93A}$ (n=52) interneurones in membrane capacitance (64±6 pF WT, 63±5 pF $SOD1^{G93A}$) and input membrane resistance (231±32 MΩ WT,

228±22 MΩ $SOD1^{G93A}$). Glycinergic postsynaptic currents (gly-PSCs) were recorded at -84 mV holding potential in the presence of CNQX (10 µM; Sigma) and SR-95531 (10 µM; Sigma). In order to detect glycinergic miniature postsynaptic currents (mPSCs), tetrodotoxin (TTX, 1 µM; Latoxan) was added. Gly-PSCs and mPSCs were abolished by application of 1 µM strychnine (Sigma).

TBOA (30 µM, Tocris Bioscience) was added to the perfusion for ≥10 minutes to deplete GABA presynaptic vesicular content.

For outside-out recordings, the same standard physiological saline solution was used as in whole-cell recordings; the pipette solution contained (in mM): 140 CsCl, 4 NaCl, 1 $MgCl_2$, 0.5 $CaCl_2$, 5 EGTA, 10 HEPES, 2 MgATP. The pH was adjusted at 7.3 (290 mOsm).

Outside-out patches were obtained in the presence of TTX (1 µM), CNQX and SR-95531 (both 10 µM) in the extracellular medium and 5 µM QX-314 in the intracellular solution and held at -84 mV. We recorded for 40 s in control solution, to make sure that the patch did not display any baseline channel openings, before applying glycine (15 µM) through the perfusion system. This glycine concentration was chosen as the most suitable one to evoke substantial receptor activation, and to avoid excessive multichannel activity that would be difficult to analyse. Under these conditions we observed at most 5 simultaneous channel openings at the beginning of the glycine application. After one minute of equilibration in glycine solution, traces were analysed for at least 30 s or as long as the quality of the recording was sufficient to allow us to measure the amplitude of openings clearly. Between 15 and 30 channel openings were measured in each trace. In noisy patches, only clear openings were considered.

Homomeric glycine receptors are known to have higher conductance than heteromers. In conditions similar to the ones we use, eg high symmetrical chloride, homomeric conductance is greater than 86 pS and heteromeric conductance is 45-54 pS, regardless the α subunit type (Bormann et al., 1993).

We classified the patches into three groups, depending on the type of channel openings they contained, namely (i) heteromeric GlyR patches, where all openings were between 4 and 5 pA (corresponding to a chord conductance of 47-59 pS), (ii) homomeric GlyR patches, where all openings were between 7 and 8 pA (83-95 pS) or (iii) mixed GlyR patches where both 4-5 pA and 7-8 pA openings was detected, suggesting the presence of a mixed population of homomeric and heteromeric receptors.

The main risk in the analysis would be to classify two simultaneous heteromeric openings as a single homomeric opening. We examined the trace at appropriate sweep speed to check whether a transition was a double event or not. If the transition appeared to be a single opening to the larger conductance, we validated the classification by further checking that it was followed by a closure of the same amplitude.

Furthermore, this error seems unlikely, given that the amplitude of homomeric openings is less than twice that of heteromeric ones: the average current amplitudes were 7.6 ± 0.3 and 4.3 ± 0.2 pA for homomeric and heteromeric openings, respectively (n= 13 patches). In traces with homomeric channels openings, we occasionally observed openings to a lower conductance (2.9 ± 0.1 pA, n=11 patches). These openings were much smaller than heteromeric openings and may represent sublevels of the homomeric conductance, as reported by Bormann et al., 1993.

For the study of motor output from the isolated spinal cord, ventral roots (VRs) of the lumbar region segments (L2 and L5) were tightly inserted, by applying a gentle negative pressure, in monopolar suction electrodes connected to Ag/Ag-Cl micropellets in glass micropipettes. Spontaneous activity was recorded also in the presence of the GABA receptor antagonist SR-95531 (10 μM) to investigate the network activity controlled by glycinergic transmission as inhibitory source. At least 10 min of recordings were used to analyse burst periodicity. Signals were amplified (DP-304 differential amplifier, Molecular Devices), digitized at 20 kHz and recorded with pCLAMP software for offline analysis.

Immunofluorescence

WT and SOD1^{G93A} cultures were fixed with 4% formaldehyde (prepared from fresh paraformaldehyde) in PBS for 60 minutes at RT and then washed in PBS. Free aldehyde groups were quenched in 0.1 M glycine in PBS for 5 minutes. The samples were blocked and permeabilized in 3% FBS, 3% BSA and 0.3% Triton-X 100 in PBS for 30 minutes at 37 ºC. Samples were incubated with primary antibodies (guinea-pig anti-glycine transporter 2 -GlyT2-, Millipore, 1:1000 and rabbit anti-glutamic acid decarboxylase 65 -GAD65-, Santa Cruz Biotechnology, 1:50) diluted in PBS with 5% FBS at 4 °C, overnight. Samples were then incubated in secondary antibodies (Alexa 488 goat anti-guinea-pig, Invitrogen, 1:400; Alexa 594 goat anti-rabbit, Invitrogen, 1:400; DAPI, Invitrogen, final concentration 5 µg/ml) for 2 h at 37 ºC and finally mounted on glass coverslips using Vectashield hardset mounting medium (Vector laboratories). For acute spinal cord slices, the same staining protocol was used, with the exception of the blocking step where a solution of 10% horse serum and 0.3% Triton-X 100 in PBS was used to enhance the penetration of the antibodies into the tissue.

Images were acquired using a Nikon C2 Confocal Microscope equipped with Ar/Kr, He/Ne, and UV lasers. Images were acquired with a 40× oil-objective (numerical aperture 1.3) using oil-mounting medium (1.515 refractive index). Confocal sections were acquired every 0.5 µm up to a total sample thickness of 12 µm. Regions of interest were confined to the ventral part of slice. Offline analysis of the image *z*-stack was performed using NIS-Elements AR software (Nikon) and the open source image-processing package, FIJI (http://fiji.sc/Fiji).

To investigate the amount of GlyT2 and GAD65 co-localization in WT and SOD1^{G93A} we used the professional image analysis software Volocity (PerkinElmer). In both channels, a threshold was set for both the intensity and the object size, thus ensuring that the observed signal indicates the presence of genuine GlyT2 and GAD65 signals. We quantified only those voxels that represented co-localized GlyT2 signals with GAD65 signals.

Statistical analysis

Results are presented as mean ± S.E., if not otherwise indicated; n= number of neurons are reported in the Figure captions. Statistically significant difference between two data sets was assessed by Student's *t* test (after checking variances homogeneity by Levene's test) for parametric data and by Mann-Whitney's test for non-parametric ones, at a minimum significance level of $P<0.05$.

Chi square test was used to assess the statistically significant differences in outside out experiments.

Results

Glycinergic synaptic currents in developing WT and SOD1^{G93A} spinal interneurons

We recorded spontaneous gly-PSCs in isolation by patch-clamping ventral interneurons from WT and SOD1^{G93A} spinal cord slices, in the presence of CNQX and SR-95531 to block PSCs mediated by AMPA/kainate and $GABA_A$ receptors (Figure 1A-B). Organotypic spinal networks mature during *in vitro* culture (Avossa et al., 2003; Furlan et al., 2007). This was reflected in WT cultures by a progressive increase in the frequency and peak amplitude of spontaneous gly-PSCs recorded at 1, 2 and 3WIV (Figure 1A, C-D). These developmental changes were similar in age-matched SOD1^{G93A} cultures (Figure 1B-D). WT and SOD1^{G93A} interneurons displayed similar values of gly-PSC frequency and amplitude in the developmental window analysed. Thus, the mean frequency values increased from 3.3±0.7 Hz at 1WIV to 11.1±0.9 Hz at 3WIV and from 1.8±0.5 Hz at 1 WIV to 11.6±1.7 Hz at 3WIV for WT and SOD1^{G93A} cultures, respectively, (Figure 1C). The mean peak amplitude values increased from 25.0±6.7 pA at 1WIV to 41.0±4.1 pA at 3WIV and from 18.6±5.3 pA to 45.7±6.6 pA for WT and SOD1^{G93A} cultures, respectively (Figure 1D).

In the next set of measurements, because of the relatively low frequency of glycinergic events at 1WIV, we focused on older ages (2 and 3 WIV) to compare the development of the kinetic properties of spontaneous gly-PSCs in WT and SOD1^{G93A} slices. It is well established that the decay of GlyR-mediated currents speeds up during physiological synaptic development, because of a switch from the expression of α2 GlyR subunits (probably forming homomeric GlyRs), to that of

the classical adult synaptic GlyR, an α1β heteromer (Malosio et al., 1991; Takahashi et al., 1992; Singer et al., 1998; Aguayo et al., 2004; Beato & Sivilotti, 2007; Lynch, 2009). The traces in Figure 2A show that this process occurs also in our explants, and that the decay time constant (τ) of gly-PSCs in both WT and $SOD1^{G93A}$ interneurons becomes progressively shorter with *in vitro* maturation. Thus, the τ value of WT gly-PSCs progressively shifted from 14.6 ±1.9 ms at the beginning of the 2WIV to 7.6±0.3 ms at the end of the 3WIV; similarly, the decay of $SOD1^{G93A}$ gly-PSCs (11.9±1.3 ms at 2 WIV) became faster at 3WIV (5.7±0.3 ms) (Figure 2A, B). In $SOD1^{G93A}$ interneurones gly-PSC appeared to decay faster than WT at 2WIV, a difference that became highly significant as the variability across neurons decreased at 3WIV (Figure 2B, ***P=0.000001). The absence of correlation between PSC rise time *vs* decay time values (Figure 2C) suggests that that differences in recording conditions, location of synapses or electronic filtering are unlikely to have affected our observations.

Figure 2D shows the measurement of the reversal potential of gly-PSCs in WT and $SOD1^{G93A}$ at 2WIV (top) and at 3WIV (bottom). The theoretical value expected for the Cl^- equilibrium potential for our intracellular and extracellular chloride concentrations is ~ -50 mV. At 2 and 3WIV the measured reversal potentials were more negative (by 5 mV and 10 mV, at 2 and 3 WIV) than the calculated one (Figure 2D). However, the reversal potential values and their shifts were identical in WT and $SOD1^{G93A}$ neurons, suggesting that local intracellular chloride concentrations are similar.

The higher gly-PSC frequency in explants after 3WIV allowed us to extend our characterisation to the properties of miniature glycinergic currents (mPSCs; recorded in the presence of TTX). The results in this group of cells (Figure 2E) confirm that WT and $SOD1^{G93A}$ mPSCs differ in their decay kinetics (mPSCs τ value: 6.9±0.3 ms WT and 5.8±0.3 ms $SOD1^{G93A}$; *P=0.035) in a manner similar to that of spontaneous gly-PSCs recorded before TTX treatment (gly-PSCs τ value: 7.0±0.4 ms WT and 5.3±0.4 ms $SOD1^{G93A}$).

The faster decay in glycinergic synaptic currents recorded in $SOD1^{G93A}$ interneurons could be due to a difference in the GlyRs that mediates these synaptic events. In order to test for this hypothesis,

in an independent set of experiments, we performed outside-out recordings from 2 and 3WIV interneurons. Figure 3A shows typical examples of such recordings, where the channel opening are downwards. While the density of channels openings was too high to allow us to measure the burst length of these channels (and compare it with the PSC decay τ), it was easy to measure the amplitude of the openings, and therefore the channel conductance. For glycine channels, conductance is a straightforward indication of the homomeric or heteromeric nature of the receptor, as it is high for homomers (greater than 86 pS in high symmetrical chloride) than for heteromers (45-54 pS, Bormann et al., 1993), irrespective of the α subunit involved. The top trace in Figure 3A is from a patch (2WIV) where the predominant channel amplitude was between 4 and 5 pA (see horizontal dashed lines). This current amplitude corresponds to a conductance of 58 pS which would suggest that the activity arises from heteromeric receptors. The bottom trace shows another patch, where the most common openings were large (7 to 8 pA), are therefore likely to stem from homomeric receptors. The middle trace shows a recording where channels with small (4 to 5 pA) and large (7 to 8 pA) amplitudes coexist, indicating the presence of a mixed population of homomeric and heteromeric receptors.

Thus patches were categorized in three populations depending on the conductances detected: ~50 pS, ~90 pS or mixed. The prevalence of the different types at different ages *in vitro* is depicted in Figure 3B. Intriguingly, at 2WIV, in WT slices 77% of patches displayed the smaller conductance, indicating a more mature GlyR expression (Takahashi et al., 1992), whereas in transgenic cultures 56% of the patches still showed mostly high conductance channel activity or a mixed population of low and high conductance channels, suggesting a delay in GlyRs maturation. This delayed maturation implies the persistence of the homomeric channels in transgenic cultures and that, if anything, should make gly-PSCs slower than WT in their decay. This was not detected, on the contrary, gly-PSCs at 2WIV appeared faster in their decay (not significant), in $SOD1^{G93A}$ explants (Figure 2B). At 3WIV the prevalence of the different conductance patterns was similar for patches

from WT and SOD1^{G93A}. This rules out the possibility that the difference in decay at 3WIV was due to large differences in the GlyRs populations expressed by the two groups (Figure 3A, B).

GABA co-release tunes glycine PSCs τ in SOD1^{G93A} spinal interneurons

During antenatal development one-third of the neurons located in the ventral spinal cord co-express glycine and GABA (Allain et al., 2006; Sibilla & Ballerini, 2009), thus we tested the ability of this amino-acid to shape gly-PSCs, by glycine displacement from GlyRs, when co-released (Lu et al., 2008). We hypothesized that the faster gly-PSCs τ in SOD1^{G93A} could be due to a delay in the maturation of glycine-GABA mixed synapses, and ultimately to the persistence of GABA co-release. GABA pre-synaptic content was depleted by TBOA (WT and SOD1^{G93A}; Mathews and Diamond, 2003) a broad-spectrum competitive antagonist of glutamate transporters (Shimamoto et al., 1998), that inhibits the glutamate uptake needed for GABA synthesis. Figure 3C-D shows that at 3WIV, TBOA treatment did not affect WT gly-PSCs decay (τ values: 8.4±0.9 ms and 9.1±1.0 ms before and after the perfusion with TBOA, respectively), but slowed down SOD1^{G93A} gly-PSCs decay (τ values: 5.7±0.5 ms and 7.4±0.8 ms before and after the addition of TBOA, respectively). The difference in decay time between the two genotypes is statistically significant before the application of TBOA (P=0.008), whereas following the treatment, the decay values become comparable (P=0.22). Our hypothesis was further supported by immunostaining experiments where we targeted GlyT2 and GAD65 to quantify the presynaptic co-localization and detect mixed glycine-GABA terminals (Dumoulin et al., 2001; Mackie et al., 2003; Dugué et al., 2005). At 3WIV co-localization of GlyT2-GAD65 is more common in transgenic cultures than in WT, and this supports our electrophysiological results (Figure 4C, E). Notably, a very similar result was obtained when we repeated the measurement in acute slices isolated from the spinal cord of WT and SOD1^{G93A} neonatal (P0) mice. GABA-glycine co-localization is more prevalent in the transgenic tissue, as shown in Figure 4A-B and D, further supporting our electrophysiological results and

validating organotypic cultures as an *in vitro* model to investigate the dynamics of maturation processes.

Bursting activity in the isolated SOD1^{G93A} neonatal spinal cord

Our observations supported the presence of a greater proportion of glycine-GABA mixed synapses in organotypic and acute SOD1^{G93A} spinal cord slices when compared to age-matched WT ones. Thus, we isolated (at P2-4 postnatal age) the entire spinal cord from WT and SOD1^{G93A} mice (n=7 and n=5, respectively) to further investigate whether MN outputs were influenced by the more prevalent GABA/glycine co-transmission. For this purpose we measured spontaneous VRs discharges. At early postnatal ages spinal cords produced sporadic and irregular discharges in 61% of WT VRs and in 87% of SOD1^{G93A}ones. In the mutant cords such discharges were characterized by significantly longer depolarizing events (Figure 5A, B; event duration: 2.8±0.2 s WT and 6.3±1.3 s SOD1^{G93A}, P=0.012). In particular, in the presence of $GABA_A$ receptor blockade, we studied MN outputs changes, potentially reflecting the faster kinetic of glycinergic synaptic events. In all WT and SOD1^{G93A} preparations, such MN outputs were transformed in robust synchronous bursts in the presence of a $GABA_A$ receptor blocker (SR-95531) used to isolate the glycinergic contribution (Figure 5C). Notably, in SOD1^{G93A} spinal cords the inter-bursts periods and the bursts duration were shorter, suggestive of an increased excitability (Figure 5D; burst duration: 27.6±3.5 s WT and 17.3±1.9 s SOD1^{G93A}, P=0.0455; inter burst period: 64.6±8.4 s WT and 39.2±3.5 s SOD1^{G93A}, P=0.0284). These results further support that tuning of inhibitory synapses is altered in SOD1^{G93A} spinal networks and that this ultimately results in important changes in the whole spinal motor output.

Discussion

Chang and Martin (2009, 2011) have shown that glycinergic inhibition of spinal MNs is impaired in the SOD1^{G93A} ALS animal model (Chang & Martin, 2009, 2011). Here we used the organotypic

cultures obtained from the same $SOD1^{G93A}$ mice to investigate developmental changes in gly-PSCs in the pre-motor spinal network of presymptomatic ALS animals (Avossa et al., 2006). We recorded from interneurons to assess how changes in the pre-motor modulation of MN activity may contribute to the early pathogenesis of ALS. Characterizing ALS animal models throughout their development is important to try to pinpoint the earliest alterations in synaptic input and neuronal excitability before the pathological process has progressed to denervation (Vinsant et al., 2013).

The present data show that, during *in vitro* development, the properties of gly-PSCs recorded from $SOD1^{G93A}$ interneurons change in a pattern similar to that reported for WT gly-PSC in cultured and *ex-vivo* samples (Gao & Ziskind-Conhaim, 1995; Gao et al., 1998; Baccei & Fitzgerald, 2004). Thus, gly-PSCs become progressively more frequent, larger in amplitude and faster in their decay. However, we found that, at 3WIV, an age in cultures roughly equivalent to early postnatal days, gly-PSCs and mPSC from ALS model mice decay faster than those from WT neurons, resulting in a reduction in charge transfer in the range of 35-20%.

In order to understand the reason for the observed difference in decay, we examined the main variables that change during development and could conceivably affect the kinetic properties of glycine receptors and therefore gly-PSC time course. First we excluded the possibility of differences in the intracellular chloride concentration that could affect gly-PSC kinetics (Pitt et al., 2008). Our measurements show that the Cl^- reversal potential was similar in the two cultures at matching *in vitro* ages. In both WT and transgenic cultures the Cl^- reversal potential differed from the predicted theoretical value. In our recording conditions it is not possible to distinguish between an impaired pipette/cell solution-exchange due to maturation dependent changes in neuronal morphology or a real shift in the internal chloride concentration due to improved extrusion (DeFazio et al 2000; Ostroumov et al., 2011). However, the detected shifts are similar in both WT and $SOD1^{G93A}$ interneurones dialysed with a 24 mM Cl^- intracellular pipette solution.

Another well-documented process that changes glycinergic inhibition in the developing CNS is the switch from the expression of $\alpha 2$ homomeric channels to that of the adult synaptic $\alpha 1\beta$ heteromeric

GlyR (Takahashi et al., 1992, Singer & Berger, 1999). Heteromeric α1β receptors have a faster deactivation (Mangin et al. 2003; Pitt et al., 2008; Krashia et al., 2011), which results in a faster decaying synaptic current (Zhang et al., 2015). Heteromeric glycine receptors have a smaller conductance than homomeric channels (Bormann et al., 1993), and thus we recorded single channel activity from outside-out patches to establish if the time course of appearance of heteromeric isoforms differed at 2 and 3 WIV in WT and SOD1^{G93A} mice. At 2 WIV the gradual shift towards the more mature receptor type appeared to be more pronounced in WT patches, but the proportion of heteromeric vs. homomeric patches was very similar at the 3WIV stage of development. These data suggest that the faster decay of SOD1^{G93A} gly-PSC cannot be due to an earlier or more complete switch to heteromeric channels. However, we must interpret these findings with caution, given that outside-out patches are likely to contain mostly extrasynaptic receptors and that by its very nature, single channel recording is not an accurate way to estimate the proportion of one type of channel *vs* the other.

We turned our attention to presynaptic processes that may affect synaptic time course. The timing of glycinergic inhibition is known to be regulated by the extent of release synchronization, which can make the PSC longer than the channel deactivation (Balakrishnan et al., 2009). Differences in release synchronization between WT and SOD1^{G93A} synapses are unlikely to explain our data, as in SOD1^{G93A} neurons the decay of gly-PSCs is faster also for unitary synaptic events (mPSCs).

This leaves the possibility that our findings are explained by differences in GABA co-release, namely that this persists longer in SOD1^{G93A} cultures. At auditory synapses, GABA co-release makes the PSC faster than the channel deactivation, by the partial agonist action of GABA on glycine receptors (Lu et al., 2008). GABA/glycine co-expression is developmentally regulated in the spinal cord, its extent decreases with development (Sibilla & Ballerini, 2009; Allain et al., 2006) and can be affected by the pattern of activity at the synapse (Nerlich et al., 2014). After depletion of GABA presynaptic content by TBOA applications (Lu et al., 2008), we indeed observed that SOD1^{G93A} gly-PSCs were no longer significantly different from WT ones in terms of decay time.

Our hypothesis was further strengthened by the detection of greater proportion of GABA-glycine mixed synapses (Dumoulin et al., 2001; Mackie et al., 2003; Dugué et al., 2005) in transgenic tissue *vs.* WT, both in cultured and in *ex vivo* spinal preparations. These results suggest that the faster decay of gly-PSC in ALS model mice is largely due the longer persistence of GABA co-release.

In developing spinal circuits, during the emergence of organized motor behaviors the fine-tuning and refinement of inhibitory neurotransmission, including the regulation of GABA/glycine co-release, are a complex, region-specific phenomenon (Jonas et al 1998; Keller et al 2001; Gonzalez-Forero & Alvarez, 2005; Sibilla & Ballerini, 2009). Here we reported for the first time that, at ages corresponding to the higher detection of GABA at glycinergic synapses in $SOD1^{G93A}$ ventral horn, the emerging motor outputs show more prolonged spontaneous bursting in $SOD1^{G93A}$ VR-recordings. This finding is consistent with the proposal of a delayed maturation of GABAergic/glycinergic inhibitory interneuronal connections (Whelan, 2003). In addition, the reduction of gly-PSC duration by the persistence of GABA/glycine co-release in $SOD1^{G93A}$ spinal cord is confirmed by the increased VR bursting, a clear symptom of increased MN pool excitability (Ballerini et al., 1999; Bracci et al., 1997), when motor outputs are recorded in the presence of a $GABA_A$ receptor antagonist.

In conclusion, the main finding of our work is that $SOD1^{G93A}$ networks display abnormal premotor network maturation long before the appearance of any symptom, and in the absence of early sign of degeneration (Avossa et al., 2006). The alteration in glycinergic inhibition might involve spinal ventral interneurons, not only MNs as previously suggested (Chang & Martin, 2009, 2011). The changes in operation of gly-PSCs may impair the optimal development of MN outputs: understanding how this occurs may provide a clearer insight into the underlying threat to MNs viability in ALS patients.

References

Aguayo LG, van Zundert B, Tapia JC, Carrasco MA, Alvarez FJ (2004) Changes on the properties of glycine receptors during neuronal development. Brain Res Rev 47, 33-45.

Allain AE, Baïri A, Meyrand P, Branchereau P (2006) Expression of the glycinergic system during the course of embryonic development in the mouse spinal cord and its co-localization with GABA immunoreactivity. J Comp Neurol 496, 832-846.

Avossa D, Rosato-Siri MD, Mazzarol F, Ballerini L (2003) Spinal circuits formation: a study of developmentally regulated markers in organotypic cultures of embryonic mouse spinal cord. Neuroscience 122, 391-405.

Avossa D, Grandolfo M, Mazzarol F, Zatta M, Ballerini L (2006) Early signs of motoneuron vulnerability in a disease model system: characterization of transverse slice cultures of spinal cord isolated from embryonic ALS mice. Neuroscience 138, 1179-1194.

Baccei ML, Fitzgerald M (2004) Development of GABAergic and glycinergic transmission in the neonatal rat dorsal horn. J Neurosci 24, 4749-4757.

Balakrishnan V, Kuo SP, Roberts PD, Trussell LO (2009) Slow glycinergic transmission mediated by transmitter pooling. Nature Neuroscience 12, 286-294

Ballerini L, Galante M (1998) Network bursting by organotypic spinal slice cultures in the presence of bicuculline and/or strychnine is developmentally regulated. Eur J Neurosci 10, 2871-2879.

Ballerini L, Galante M, Grandolfo M, Nistri A (1999) Generation of rhythmic patterns of activity by ventral interneurons in rat organotypic spinal slice culture. J Physiol 517, 459-475.

Bracci E, Ballerini L, Nistri A (1996) Spontaneous rhythmic bursts induced by pharmacological block of inhibition in lumbar motoneurons of the neonatal rat spinal cord. J Neurophysiol 75, 640-647.

Bracci E, Beato M, Nistri A. (1997) Afferent inputs modulate the activity of a rhythmic burst generator in the rat disinhibited spinal cord in vitro. J Neurophysiol. 77, 3157-3167.

Beato M, Nistri A (1999) Interaction between disinhibited bursting and fictive locomotor patterns in the rat isolated spinal cord. J Neurophysiol 82, 2029-2038.

Beato M, Sivilotti LG (2007) Single-channel properties of glycine receptors of juvenile rat spinal motoneurones in vitro. J Physiol 580, 497-506.

Ben-Ari Y (2008) Neuro-archaeology: pre-symptomatic architecture and signature of neurological disorders. Trends Neurosci 31, 626-36.

Bormann J, Rundstrom N, Betz H, Langosch D (1993) Residues within transmembrane segment M2 determine chloride conductance of glycine receptor homo- and hetero-oligomers EMBO J 12, 3729–3737.

Chang Q, Martin LJ (2009) Glycinergic innervation of motoneurons is deficient in amyotrophic lateral sclerosis mice: a quantitative confocal analysis. Am J Pathol 174, 574-585.

Chang Q, Martin LJ (2011) Glycine receptor channels in spinal motoneurons are abnormal in a transgenic mouse model of amyotrophic lateral sclerosis. J Neurosci 31, 2815-2827.

Cirulli ET, Lasseigne BN, Petrovski S, Sapp PC, Dion PA, et al (2015) Exome sequencing in amyotrophic lateral sclerosis identifies risk genes and pathways. Science 347, 1436-41

Clements JD, Bekkers JM (1997) Detection of spontaneous synaptic events with an optimally scaled template. Biophys J 73, 220-229.

Copray JC, Jaarsma D, Kust BM, Bruggeman RW, Mantingh I, Brouwer N, Boddeke HW. (2003) Expression of the low affinity neurotrophin receptor p75 in spinal motoneurons in a transgenic mouse model for amyotrophic lateral sclerosis. Neuroscience 116, 685-94.

DeFazio RA, Keros S, Quick MW, Hablitz JJ. (2000) Potassium-coupled chloride cotransport controls intracellular chloride in rat neocortical pyramidal neurons. J Neurosci. 20, 8069-76.

Dugué GP, Bumoulin A, Triller A, Dieudonné S (2005) Target-dependent use of coreleased inhibitory transmitters at central synapses. J Neurosci 25, 6490-6498.

Dumoulin A, Triller A, Dieudonné S (2001) IPSC kinetics at identified GABAergic and mixed GABAergic and glycinergic synapses onto cerebellar golgi cells. J Neurosci 21, 6045-6057.

Furlan F, Guasti L, Avossa D, Becchetti A, Cilia E, Ballerini L, Arcangeli A (2005) Interneurons transiently express the ERG K^+ channels during development of mouse spinal networks in vitro. Neuroscience 135, 1179-1192.

Furlan F, Taccola G, Grandolfo M, Guasti L, Arcangeli A, Nistri A, Ballerini L (2007) ERG conductance expression modulates the excitability of ventral horn GABAergic interneurons that control rhythmic oscillations in the developing mouse spinal cord. J Neurosci 27, 919-928.

Galante M, Nistri A, Ballerini L (2000) Opposite changes in synaptic activity of organotypic rat spinal cord cultures after chronic block of AMPA/kainate or glycine and $GABA_A$ receptors. J Physiol 523, 639-651.

Gao BX, Ziskind-Conhaim (1995) Development of glycine- and GABA-gated currents in rat spinal motoneurons. J Neurophysiol 74, 113-121.

Gao BX, Cheng G, Ziskind-Conhaim L (1998) Development of spontaneous synaptic transmission in the rat spinal cord. Neurophysiol 79, 2277-2287.

González-Forero D, Alvarez FJ. (2005) Differential postnatal maturation of $GABA_A$, glycine receptor, and mixed synaptic currents in Renshaw cells and ventral spinal interneurons. J Neurosci. 25, 2010-23.

Gurney ME, Pu H, Chiu AY, Dal Canto MC, Polchow CY, Alexander DD, Caliendo J, Hentati A, Kwon YW, Deng HX, Chen W, Zhai P, Sufit RL, Siddique T (1994) Motor neuron degeneration in mice that express a human Cu,Zn superoxide dismutase mutation. Science 264, 1772-1775.

Holasek SS, Wengenack TM, Kandimalla KK, Montano C, Gregor DM, Curran GL, Poduslo JF (2005) Activation of the stress−activated MAP kinase, p38, but not JNK in cortical motor neurons during early presymptomatic stages of amyotrophic lateral sclerosis in transgenic mice. Brain Res 1045, 185−98.

Keller AF, Coull JA, Chery N, Poisbeau P, De Koninck Y. (2001) Region-specific developmental specialization of GABA-glycine cosynapses in laminas I-II of the rat spinal dorsal horn. J Neurosci. 21, 7871-80.

Krashia P, Lape R, Lodesani F, Colquhoun D, Sivilotti LG (2011) The long activations of α2 glycine channels can be described by a mechanism with reaction intermediates ("flip"). J Gen Physiol 137, 197-216.

Jonas P, Bischofberger J, Sandkühler J. (1998) Corelease of two fast neurotransmitters at a central synapse. Science, 281, 419-24.

Ling SC, Polymenidou M, Cleveland DW (2013) Converging mechanisms in ALS and FTD: disrupted RNA and protein homeostasis. Neuron 79, 416-38.

Lynch JW (2009) Native glycine receptor subtypes and their physiological roles. Neuropharmacology 56, 303-309.

Lu T, Rubio ME, Trussell LO (2008) Glycinergic transmission shaped by corelease of GABA in a mammalian auditory synapse. Neuron 57, 524-535.

Mackie M, Hughes DI, Maxwell DJ, Tillakaratne NJ and Todd AJ (2003) Distribution and colocalisaztion of glutamate decarboxylase isoforms in the rat spinal cord. Neurosci 119, 461-472.

Malosio ML, Marqueze-Pouey B, Kuhse J, Betz H (1991) Widespread expression of glycine receptor subunit mRNAs in the adult and developing rat brain. EMBO J 10, 2401-2409.

Mangin JM, Baloul M, Prado De Carvalho L, Rogister B, Rigo JM, Legendre P (2003) Kinetic properties of the alpha2 homo-oligomeric glycine receptor impairs a proper synaptic functioning. J Physiol 553, 369-86.

Martin LJ, Chang Q (2012) Inhibitory synaptic regulation of motoneurons: a new target of disease mechanisms in amyotrophic lateral sclerosis. Mol Neurobiol 45, 30-42.

Mathews GC, Diamond JS (2003) Neuronal glutamate uptake contributes to GABA synthesis and inhibitory synaptic strength. J Neurosci 23, 2040-2048.

McGoldrick P, Joyce PI, Fisher EM, Greensmith L (2013) Rodent models of amyotrophic lateral sclerosis. Biochim Biophys Acta 1832, 1421-1436.

Nerlich J, Kuenzel T, Keine C, Korenic A, Rübsamen R, Milenkovic I (2014) Dynamic fidelity control to the central auditory system: synergistic glycine/GABAergic inhibition in the cochlear nucleus. J Neurosci 34, 11604-11620.

Nigro A, Menon R, Bergamaschi A, Clovis YM, Baldi A, Ehrmann M, Comi G, De Pietri Tonelli D, Farina C, Martino G, Muzio L (2012). MiR-30e and miR-181d control Radial Glia cell proliferation via HtrA1 modulation. Cell Death Dis 3, e360.

Ostroumov A, Simonetti M, Nistri A. (2011). Cystic fibrosis transmembrane conductance regulator modulates synaptic chloride homeostasis in motoneurons of the rat spinal cord during neonatal development. Dev Neurobiol. 71, 253-268.

Pitt SJ, Sivilotti LG, Beato M (2008) High intracellular chloride slows the decay of glycinergic currents. J Neurosci 28, 11454-11467.

Rao SD, Yin HZ, Weiss JH (2003) Disruption of glial glutamate transport by reactive oxygen species produced in motor neurons. J Neurosci 23, 2627−33.

Robberecht W, Philips T (2013) The changing scene of amyotrophic lateral sclerosis. Nat Rev Neurosci 14, 248-264.

Rosato-Siri MD, Zoccolan D, Furlan F, Ballerini L (2004) Interneurone bursts are spontaneously associated with muscle contractions only during early phases of mouse spinal network development: a study in organotypic cultures. Eur J Neurosci 20, 2697-2710.

Rothstein JD (2003) Of mice and men: reconciling preclinical ALS mouse studies and human clinical trials. Ann Neurol 53, 423-426.

Rothstein JD (2009) Current hypotheses for the underlying biology of amyotrophic lateral sclerosis. Ann Neurol 65 Suppl 1, S3-9.

Shimamoto K, LeBrun B, Yasuda-Kamatani Y, Sakaitani M, Shigeri Y, Yumoto N, Nakajima T (1998) DL-threo-β-benzyloxyaspartate, a potent blocker of excitatory amino acid transporters. Mol Pharmacol 53, 195-201.

Schutz B (2005) Imbalanced excitatory to inhibitory synaptic input precedes motor neuron degeneration in an animal model of amyotrophic lateral sclerosis. Neurobiol Dis 20, 131-40.

Sibilla S, Ballerini L (2009) GABAergic and glycinergic interneuron expression during spinal cord development: dynamic interplay between inhibition and excitation in the control of ventral network outputs. Progress Neurobiol 89, 46-60.

Singer JH, Talley EM, Bayliss DA, Berger AJ (1998) Development of glycinergic synaptic transmission of rat brain stem motoneurons. J Neurophysiol 80, 2608-2620.

Singer JH, Berger AJ (1999) Contribution of single-channel properties to the time course and amplitude variance of quantal glycine currents recorded in rat motoneurons. J Neurophysiol 81, 1608-1616.

Streit J, Spenger C, Lüscher HR (1991) An organotypic spinal cord - dorsal root ganglion - skeletal muscle coculture of embryonic rat. II. Functional evidence for the formation of spinal reflex arcs in vitro. Eur J Neurosci 3, 1054-1068.

Taccola G, Margaryan G, Mladinic M, Nistri A (2008) Kainate and metabolic perturbation mimicking spinal injury differentially contribute to early damage of locomotor networks in the *in vitro* neonatal rat spinal cord. Neurosci 155, 538-555.

Takahashi T, Momiyama A, Hirai K, Hishinuma F and Akagi H (1992) Functional correlation of fetal and adult forms of glycine receptors with developmental changes in inhibitory synaptic receptor channels. Neuron 9, 1155-1161.

Turner BJ, Talbot K (2008) Transgenics, toxicity and therapeutics in rodent models of mutant SOD1-mediated familial ALS. Prog Neurobiol 85, 94-134.

Veeraraghavan P, Nistri A (2015) Modulatory effects by CB1 receptors on rat spinal locomotor networks after sustained application of agonists or anatagonists. Neurosci 303, 16-33.

Vinsant S, Mansfield C, Jimenez-Moreno R, Del Gaizo Moore V, Yoshikawa M, Hampton TG, Prevette D, Caress J, Oppenheim RW, Milligan C (2013) Characterization of early pathogenesis in the SOD1(G93A) mouse model of ALS: part I, background and methods. Brain Behav. 3, 335-50.

Whelan PJ. (2003) Developmental aspects of spinal locomotor function: insights from using the in vitro mouse spinal cord preparation. J Physiol. 553, 695-706.

Zhang Y, Dixon CL, Keramidas A, Lynch JW (2015) Functional reconstitution of glycinergic synapses incorporating defined glycine receptor subunit combinations. Neuropharmacology 89, 391-397.

Competing interests

The authors declare no competing financial interests.

Author Contributions

M.M. and V.R. performed synaptic electrophysiology and all the experimental analysis on slice cultures; M.M. and P.V. performed spinal cord VR recordings; M.M. and J.L. design and performed immunofluorescence, confocal microscopy and the image analysis on acute and cultured spinal slices; G.C. performed and analyzed single channel electrophysiology; C.R. and L.M. performed acute slices isolation and processing for the histology; L.S. design single channel experiments, drafted and revised the MS critically for important intellectual content; L.B. conceived the study, designed the experiments, designed and contributed to the analysis of data and wrote the manuscript. All authors discussed the results and approved the final version of the manuscript and agree to be

accountable for all aspects of the work in ensuring that questions related to the accuracy or integrity of any part of the work are appropriately investigated and resolved; all persons designated as authors qualify for authorship, and all those who qualify for authorship are listed.

Funding

We acknowledge financial support from the NEUROSCAFFOLDS-FP7-NMP-604263 and PRIN-MIUR n. 2012MYESZW. G. Cellot was supported by the *Fondazione Alberto and Kathleen Casali*, Trieste, Italy.

Acknowledgements

We are especially grateful to Prof Andrea Nistri for his helpful comments and for supervising the entire spinal cord experiments and to Dr. Micaela Grandolfo for supervising the immune staining and its quantification.

Figures and Legends

Figure 1. WT and $SOD1^{G93A}$ ventral interneurons display similar developmental regulation in gly-PSCs frequency and amplitude. **A,** Representative traces of spontaneous gly-PSCs recorded at 2WIV (top) and 3WIV (bottom) in WT and **B,** in aged matched $SOD1^{G93A}$. **C,** Plots of gly-PSCs frequency and **D,** amplitudes values for WT (black) and $SOD1^{G93A}$ (grey) interneurons, note the changes brought about by *in vitro* maturation (total number of neurons were n= 93 WT and n=76 $SOD1^{G93A}$, with ≥400 PSCs analysed per cell; divided by DIV: 9-12 DIV n=4 WT and n=5 $SOD1^{G93A}$, 13-14 DIV n=6 WT and n=10 $SOD1^{G93A}$, 15-16 DIV n=12 WT and n=10 $SOD1^{G93A}$, 17-19 DIV n=33 WT and n=31 $SOD1^{G93A}$, 20-22 DIV n=38 WT and n=20 $SOD1^{G93A}$).

Figure 2. $SOD1^{G93A}$ gly-PSCs decay faster than WT gly-PSC after *in vitro* development. **A,** Superimposed traces show pharmacologically isolated gly-PSCs recorded from WT (left) and $SOD1^{G93A}$ (middle) ventral interneurones at 2WIV (top row) and 3WIV (bottom row; average PSCs to the side). The traces to the right of the panel are WT (black) and $SOD1^{G93A}$ (grey) average traces

superimposed and scaled to the peak, in order to highlight the different decay time. **B,** Plot of the changes in the decay time constant (τ) during *in vitro* growth (overall n=74 WT and n=52 $SOD1^{G93A}$; divided by DIV: 13-14 DIV n=6 WT and n=10 $SOD1^{G93A}$, 15-16 DIV n=12 WT and n=10 $SOD1^{G93A}$, 17-19 DIV n=26 WT and n=16 $SOD1^{G93A}$, 20-22 DIV n=30 WT and n=16 $SOD1^{G93A}$). **C**, scatter plot of rise time *versus* decay time; in both WT and $SOD1^{G93A}$ at 3WIV (n=56 WT and n=32 $SOD1^{G93A}$) regression analysis reveals no linear relationship between these two parameters (r=0.2344, probability=0.095 and r=0.3435, probability=0.093 for WT and $SOD1^{G93A}$ neurons, respectively). **D**, The I-V curves were obtained by plotting gly-PSCs mean amplitude against Vh at 2WIV (top) and 3WIV (bottom) for WT and $SOD1^{G93A}$ ventral interneurons (n=31 cells WT and n=23 cells $SOD1^{G93A}$). Note that the calculated reversal potential was ~ -55 mV at 2WIV and ~ -60 mV at 3WIV. **E**, Superimposed individual WT and $SOD1^{G93A}$ gly-mPSCs, and average mPSCs (top row). The estimated average gly-PSC and mPSC charges (area under the curve) were: in WT 459.7±83.4 pA×ms and 170.2±19.5 pA×ms, PSCs and mPSCs respectively; in $SOD1^{G93A}$ 294.9±33.2 pA×ms and 139.5±15.2 pA×ms, PSCs and mPSCs, respectively. Bottom row: box plots of the decay time constants of WT and $SOD1^{G93A}$ glycinergic PSCs and mPSCs (n=14 WT and n=10 $SOD1^{G93A}$); superimposed average and scaled tracings are gly-PSCs (left) and gly-mPSCs (right) for WT (black) and $SOD1^{G93A}$ (grey). * $P<0.05$; ** $P< 0.01$; *** $P< 0.001$.

Figure 3. GlyR-mediated single-channel activity in outside-out WT and $SOD1^{G93A}$ patches and contribution of GABA co-release in shaping spontaneous gly-PSCs in WT and $SOD1^{G93A}$ synapses. **A,** Representative current traces from outside-out patches with low or high conductances (top and bottom, respectively), and for a patch with a mixed population of conductances (middle). Dashed lines represent diverse amplitude of channel opening for different receptor types. Channel openings were elicited by bath application of glycine (15 μM) at a Vh of −84 mV. **B**, Proportion of patches in the three conductance categories (~50 pS, mixed, ~90 pS) at 2 (n=82) and 3WIV (n=23) in WT and

SOD1^{G93A}. **C**, Representative traces of spontaneous WT (left) and SOD1^{G93A} (right) gly-PSCs before (top row) and after (bottom row) TBOA (30 μM) application. The superimposed glycinergic events and their average trace (to the right) are depicted below each recording. **D**, Box plot summary of the WT and SOD1^{G93A} mean decay time constant values for gly-PSCs before and after TBOA application (n=7 WT and n=13 SOD1^{G93A}); WT (black) and SOD1^{G93A} (grey) gly-PSCs averaged traces are scaled and superimposed in the absence (left) and in the presence (right) of TBOA. * $P<0.05$; ** $P< 0.01$.

Figure 4. Co-localization of GlyT2 and GAD65 immunostainings in the WT and SOD1^{G93A} immature spinal cord. **A**, Confocal images of the ventral horn of WT and SOD1^{G93A} acute spinal slices isolated from neonatal (P0) mice and stained for GlyT2 (in green) and GAD65 (in red). **B**, Confocal high magnification of a region (from A) showing the appearance of GlyT2 (in green) and GAD65 (in red) clusters. Co-localization of GlyT2 (in green) and GAD65 (in red) clusters identify mixed synapses. **C**, Organotypic cultures: confocal high magnification of the ventral area of WT (left) and SOD1^{G93A} (right) cultured slices at 3WIV, similarly to the acute ones, co-localization of GlyT2 (in green) and GAD65 (in red) clusters identify mixed synapses. In **D** and **E**, Box plots show co-localized GlyT2 and GAD65 clusters are more common in SOD1^{G93A} (grey) spinal slices than in WT slices (black). This was seen both in acute slices (P0, **D**, n=number of ROIs, n=12 WT and n=12 SOD1^{G93A}) and in cultured slices (3WIV **E**, n=number of ROIs, n=12 WT and n=12 SOD1^{G93A}). Scale bars: 50 μm in **A,** 10 μm in **B** and **C**. * $P<0.05$

Figure 5. Motor outputs in WT and SOD1^{G93A} spinal cords isolated from P3 old mice. **A,** Representative traces of spontaneous activity simultaneously recorded from left (l) and right (r) lumbar ventral roots 5 (LVR5) and 2 (LVR2) in WT (top) and SOD1^{G93A} (bottom) spinal cords. **B,** Box plots of event duration for WT (black, n=7) and SOD1^{G93A} (grey, n=5) spinal cord preparations. **C,** Representative traces of VRs activity recorded in the presence of SR-95531 in WT (top) and

SOD1^{G93A} (bottom) spinal cords. **D,** Box plots of burst duration and inter burst period in WT (black, n=7) and SOD1^{G93A} (grey, n=5) mice.

E, confocal images of ventral horn of WT (left) and SOD1^{G93A} (right) spinal cords (same preparations as recorded in B), the co-localization of GlyT2 (in green) and GAD65 (in red) clusters identify mixed synapses. **F,** Box plots show the greater co-localization of GlyT2 and GAD65 clusters in SOD1^{G93A} spinal tissue (same preparations as recorded in B; n=number of ROIs, n=5 WT and n=5 SOD1^{G93A}). Scale bar: 50 μm. * $P<0.05$.

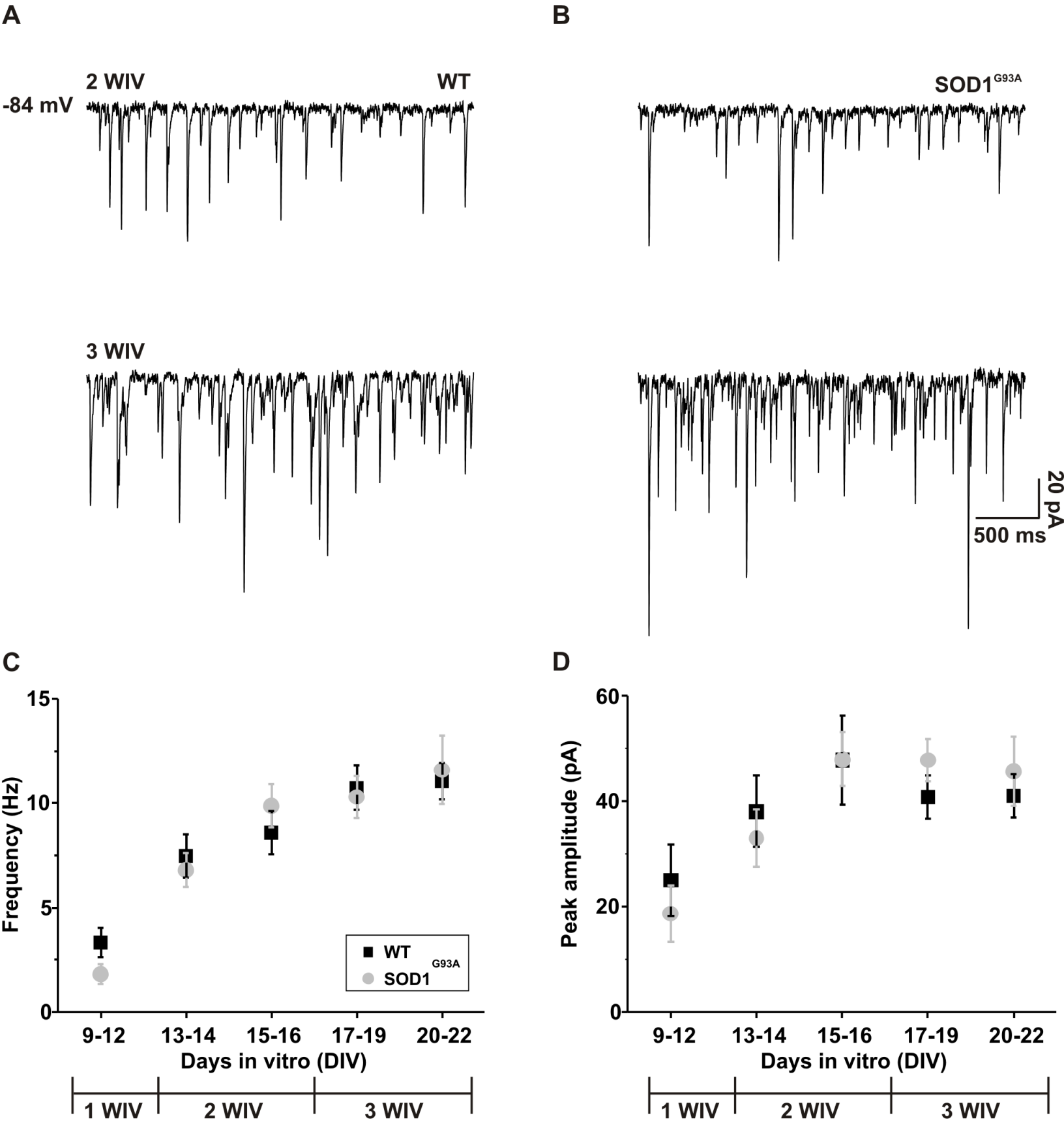
A
B
2 WIV
WT
-84 mV
SOD1G93A
3 WIV
20 pA
500 ms
C
D
Frequency (Hz)
Peak amplitude (pA)
WT
SOD1G93A
9-12
13-14
15-16
17-19
20-22
Days in vitro (DIV)
1 WIV
2 WIV
3 WIV

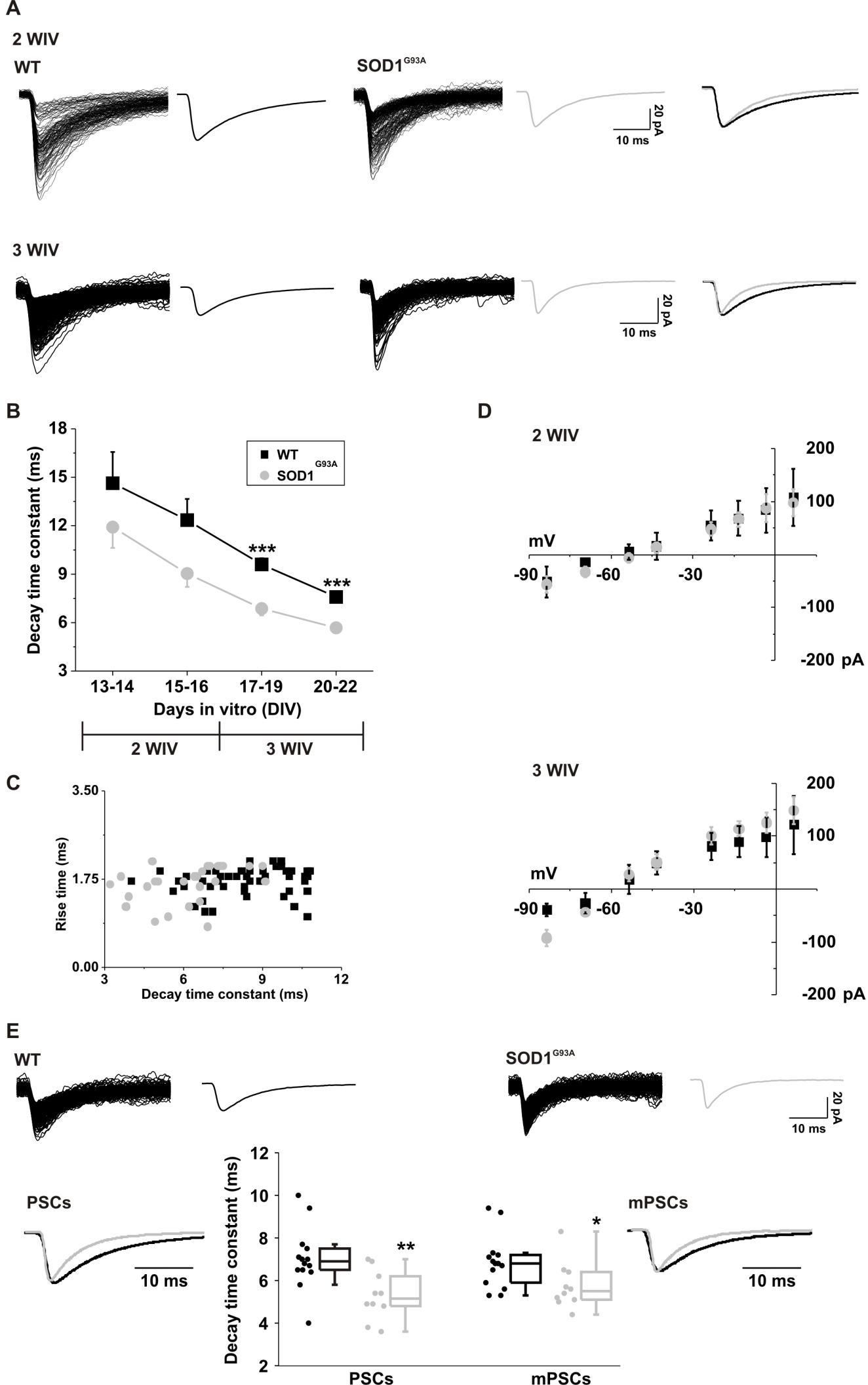
A
2 WIV
WT
SOD1G93A
20 pA
10 ms
3 WIV
20 pA
10 ms
B
Decay time constant (ms)
WT
G93A
SOD1
***
***
13-14
15-16
17-19
20-22
Days in vitro (DIV)
2 WIV
3 WIV
C
Rise time (ms)
Decay time constant (ms)
D
2 WIV
mV
-90
-60
-30
200
100
-100
-200 pA
3 WIV
mV
-90
-60
-30
200
100
-100
-200 pA
E
WT
SOD1G93A
20 pA
10 ms
PSCs
10 ms
Decay time constant (ms)
**
*
PSCs
mPSCs
mPSCs
10 ms

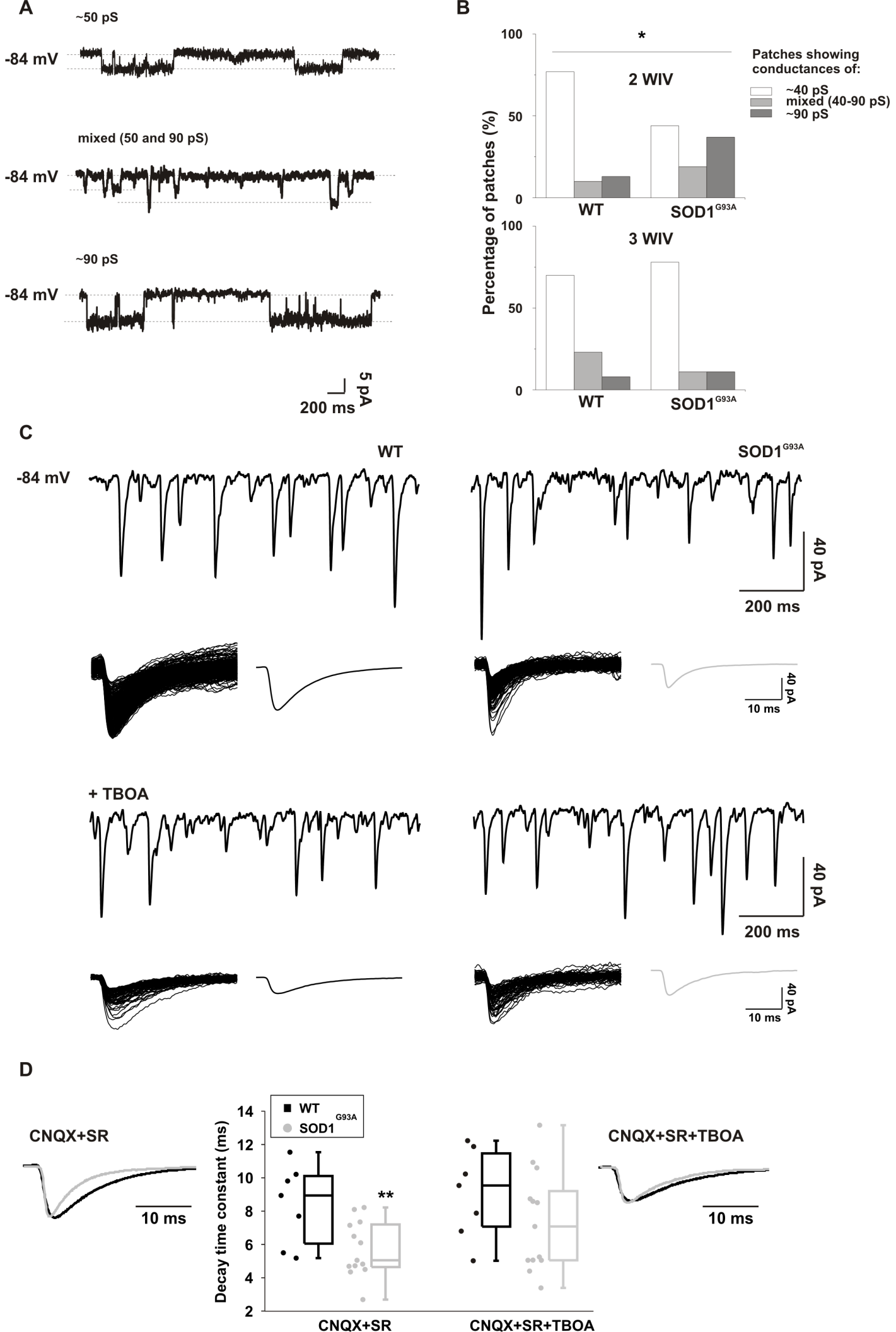
A
~50 pS
-84 mV
mixed (50 and 90 pS)
-84 mV
~90 pS
-84 mV
5 pA
200 ms
B
100
50
0
*
2 WIV
Patches showing conductances of:
~40 pS
mixed (40-90 pS)
~90 pS
Percentage of patches (%)
WT
SOD1G93A
100
50
0
3 WIV
WT
SOD1G93A
C
WT
SOD1G93A
-84 mV
40 pA
200 ms
40 pA
10 ms
+ TBOA
40 pA
200 ms
40 pA
10 ms
D
CNQX+SR
10 ms
WT
SOD1G93A
Decay time constant (ms)
14
12
10
8
6
4
2
**
CNQX+SR
CNQX+SR+TBOA
CNQX+SR+TBOA
10 ms

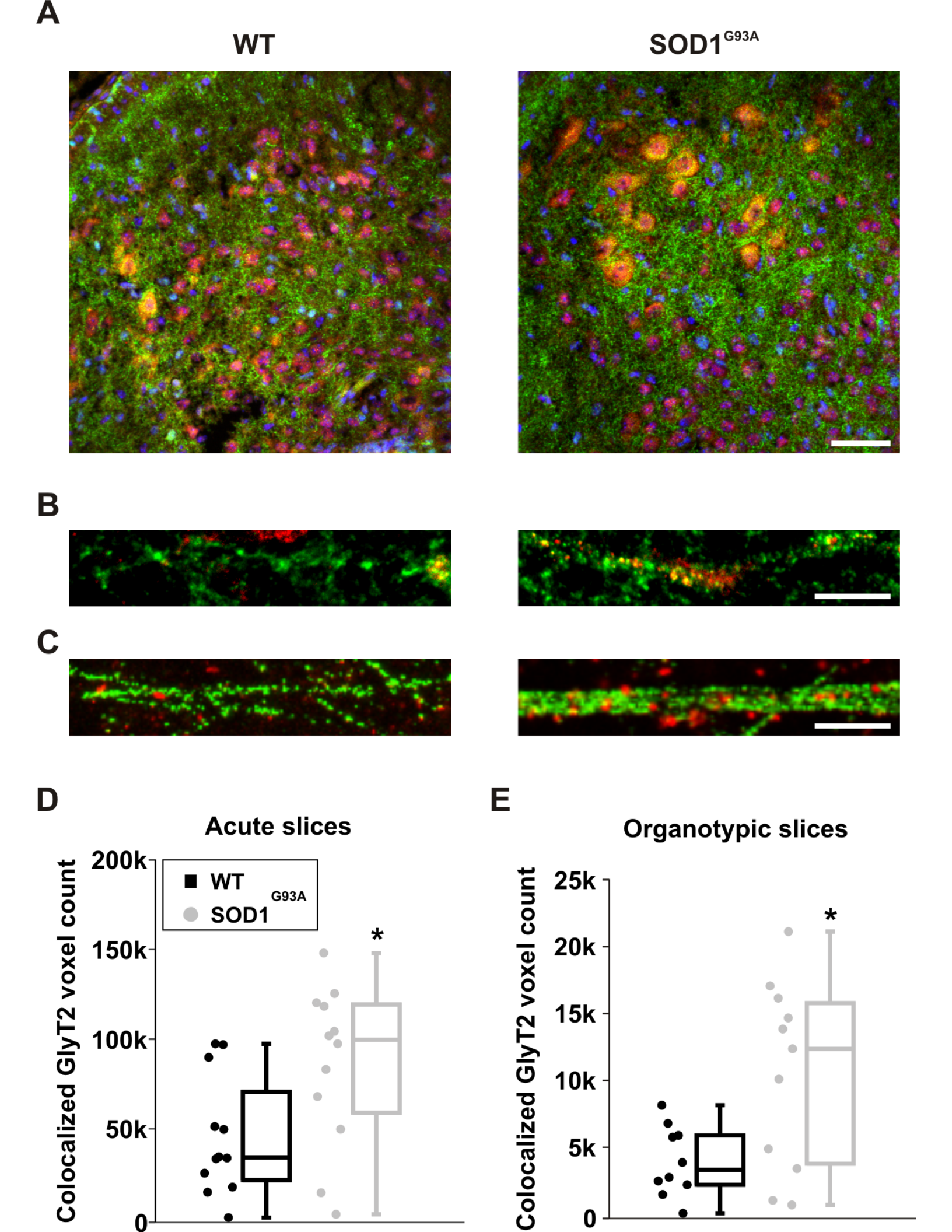
A
WT
SOD1G93A
B
C
D
Acute slices
Colocalized GlyT2 voxel count
200k
150k
100k
50k
0
WT
G93A
SOD1
*
E
Organotypic slices
Colocalized GlyT2 voxel count
25k
20k
15k
10k
5k
0
*

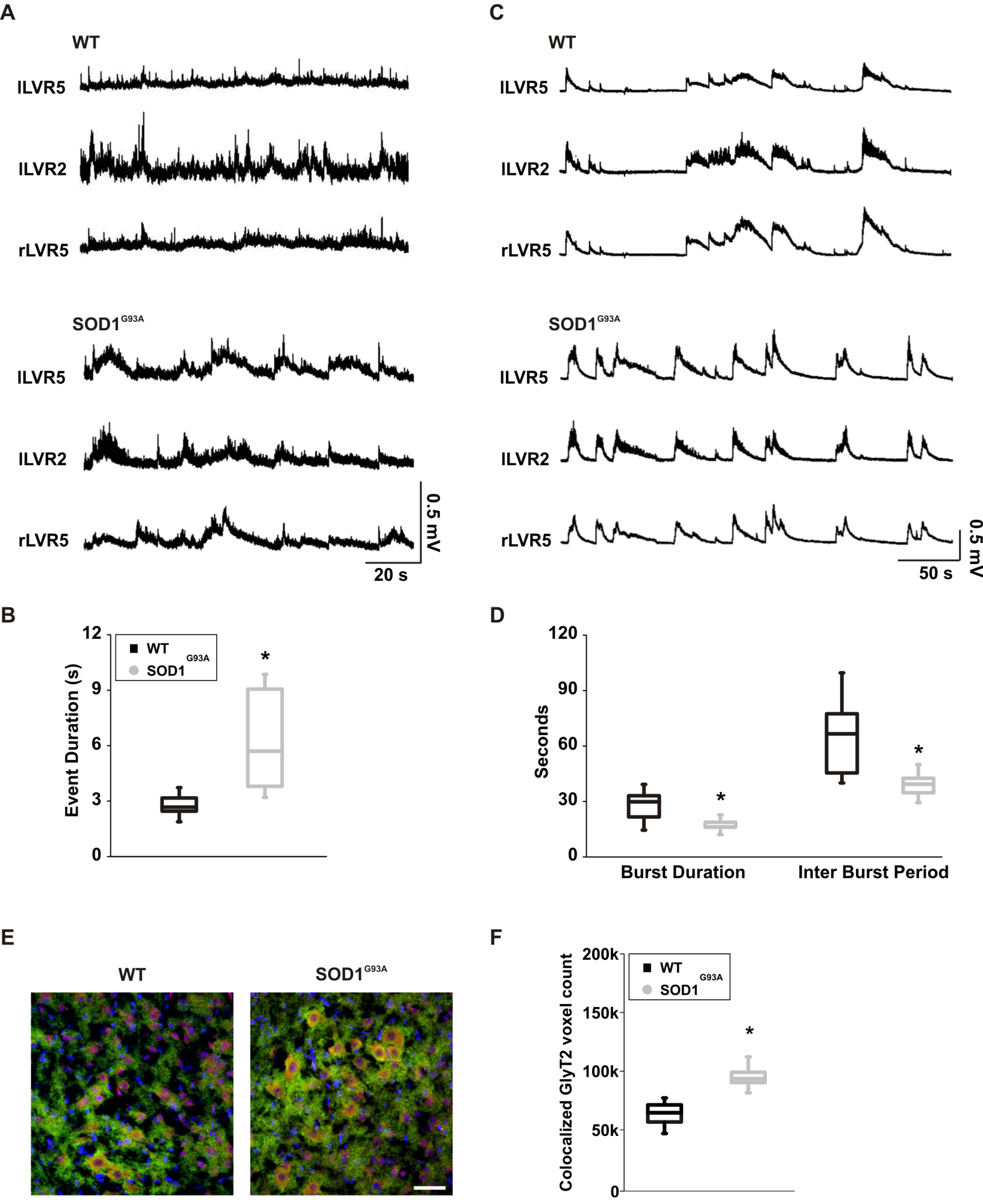
A
WT
ILVR5
ILVR2
rLVR5
SOD1G93A
ILVR5
ILVR2
rLVR5
0.5 mV
20 s
C
WT
ILVR5
ILVR2
rLVR5
SOD1G93A
ILVR5
ILVR2
rLVR5
0.5 mV
50 s
B
Event Duration (s)
12
9
6
3
0
WT
G93A
SOD1
*
D
Seconds
120
90
60
30
0
*
*
Burst Duration
Inter Burst Period
E
WT
SOD1G93A
F
Colocalized GlyT2 voxel count
200k
150k
100k
50k
0
WT
G93A
SOD1
*